IOSR Journal of Applied Physics (IOSR-JAP)
e-ISSN: 2278-4861.Volume 9, Issue 6 Ver. I (Nov. - Dec. 2017), PP 23-33
www.iosrjournals.org

Narrow Visible Emission And Narrowing Band Gap In Ho^{3+}-Co Doped Y_2O_3: Eu^{3+} Nanopowders Prepared Via Sol- Combustion Route

Abdub G. Ali*[1], Francis B. Dejene[2],Hendrik C. Swart[3]
*[1]Department of Physical Sciences, School of Pure and Applied Sciences, Meru University of Science and Technology, P.O.Box 972, Meru , Kenya
[2]Physics Department, University of the Free State, Private Bag X13, Phuthaditjhaba ,South Africa
[3]Physics Department, University of the Free State, P.O. Box 339, Bloemfontein South Africa
Corresponding Author: Abdub G. Ali**

Abstract: *Nanocrystalline Eu^{3+}, Ho^{3+} co-doped Y_2O_3 powders with a maximum size of 9.8 nm were prepared by the sol-combustion process, using Y $(NO_3).6HO_2$ as an oxidizer, europium and holonium nitrates as activators, thiourea as a fuel and ethanol as a solvent. The crystal structure and optical properties were investigated by X-ray diffraction (XRD) patterns, Scanning electron microscope (SEM), equipped with energy dispersive X-ray (EDX), Ultra-violet visible (UV-Vis) spectroscopy, and Photoluminescence (PL). As Holonium concentration (x) varies from x = 0.1 to 0.5, the Y_2O_3:Eu^{3+}:Ho^{3+} nanopowder exhibits a body – centred cubic structure of Y_2O_3 without any significant formation of a separated EuO_2, or Ho_2O_3 phase. UV-Vis reveals that the optical band gap of Y_2O_3:Eu^{3+}:$Ho^{3+}{}_x$ alloys show red shift with increase in x. With increase in Ho concentration (x), the PL spectra show several narrow visible light emission outspreading from 450 to 650 nm with monotonous red shift attributed to both the intrinsic Y_2O_3:Eu^{3+}: $Ho^{3+}{}_x$ property and the introduction of vast crystalline defects due to the high concentration of Ho^{3+} substitution. The presence of Eu^{3+} and Ho^{3+} impurities in the Y_2O_3 structure induced the formation of new recombination centres with lower emission energies and shows direct modulation of band gap. This method has proven to be ideal and simple to synthesize material for devices operating in the visible region as well as for developing heterojunction structures for optoelectronic device applications with desired efficiency.*

PACS numbers: *Valid PACS appear here*
Keywords: *Y_2O_3:Eu^{3+}: $Ho^{3+}{}_x$, band gap, sol-combustion, narrow emission, Fermi level*

Date of Submission: 30-10-2017 Date of acceptance: 16-11-2017

I. Introduction

Potential applications in environmental sciences, medicine, photolithography, material processing, and high-density optical data storage have stimulated the development of solid-state lasers working in the ultraviolet (UV) spectral range [1,2]. Frequency upconversion (UC) is one method to produce short wavelength laser, pumped with relatively longer wavelength laser through intrinsic energy level matching of certain rare-earth ions [3]. Traditional visible lasers, such as argon-krypton lasers, are expensive, bulky and complex in structure. These shortcomings greatly restrict the development of such lasers for practical applications. In recent years, the development of commercial solid state Nd^{3+} lasers has made significant progress. High-power and cost-effective compact 532-nm continuous wave (CW) solid state laser is now readily available. More importantly, the energy of such green laser matches well with the energy structures of trivalent holmium ions so that the green laser can resonate with the thermalized $^5S_2/^5F_4$ states [4].

On other hand, luminescent nanocrystals (NCs) doped with rare earth ions were paid more attentions because of their interesting luminescent properties. They can be used as components in displays [5], light emitting diodes [6], biological assays [7], and optoelectronic devices [8]. Cubic Y_2O_3:Eu^{3+} is one of the most important commercial red phosphors, which can be used in fluorescent lights, cathode ray tubes (CRTS), plasma display panel (PDP), and field emission display (FED) [9]. Yttrium oxide (Y_2O_3) has been investigated widely as a host material for rare-earth ion doping in optical applications [10] on account of its excellent chemical stability, broad transparency range (0.2 to 8μm) with a band gap of 5.6 eV, high refractive index, and low phonon energy [11-13]. Furthermore, the similarities in the chemical properties and ionic radius of RE ions and Y_2O_3 make it an attractive choice as a host material [14, 15]. Many methods for synthesis of Y_2O_3:Eu^{3+}:Ho^{3+} phosphor has been reported, including sol-gel method [16], spray pyrolysis method [17], hydrothermal method [18], and precipitation method [19]. Wet chemical methods have been widely developed to prepare the luminescent materials [20], since these processes have advantages of good homogeneity through mixing the

starting materials at the molecular level in solution, a lower calcination temperature and a shorter heating time. However, sol-gel process often requires expensive and environmentally unfriendly organic precursors and solvents. Then a simple technique, sol- combustion synthesis, is beginning to attract a great deal of interest. Sol-combustion is one of the simplest and most versatile approaches available to obtain single-phase powders at low temperatures with shorter reaction times and little residual impurities as compared with conventional solid-state reactions [21].

Trivalent holmium ion (Ho^{3+}) has many long-lived intermediate metastable levels, from which excited state absorption (ESA) can take place [22, 23]. There are also several high-lying metastable levels that can give rise to transitions at various wavelengths in the visible and UV regions [9]. Most studies on Ho^{3+}-doped materials were mainly focused on infrared and visible regions. There are also a few papers devoted to the studies of UV and violet fluorescence under IR or red laser excitation [5, 7, 10, and 11]. Here we report the generation of yellow, orange and red luminescence spectra in the range of 450 - 650 nm in Y_2O_3:Eu^{3+}: Ho^{3+} ceramic.

II. Experimental

2.1 Nanocrystals synthesis

All the chemicals used for the preparation of the powders were of analytical grade. In the present study Y $(NO_3).6HO_2$ is used as an oxidizer, thiourea employed as a fuel and Eu^{3+} and Ho^{3+} as activators. Y $(NO_3)_3.6H_2O$, Ho $(NO_3)_3{\cdot}6H_2O$ and Eu $(NO_3).6H_2O$ with proportional molar ratios of cations were completely dissolved in de-ionized water by constant rate stirring at 80 ◦C. Subsequently, citric acid was added into the solution with 1:3 molar ratios of (Y+ Ho+Eu) to citric acid. After complete dissolution, the pH of the solution was adjusted to 6.0 by the addition of ammonium hydroxide. The solution was then introduced into a muffle furnace preheated to 500^0c. After about 10 minutes the solution boiled and was ignited to a self-propagating flame. The fluffy black bulk obtained was crushed and then calcined at 900 ◦C for 4 h in air to remove remaining organic additives so that the nanocrystals were formed. These nanocrystals were pressed under 10 MPa pressure into a smooth and flat disk, then sintered at 1200 ◦C for 36 h in air to form ceramic samples.

2.2 Characterization

To determine the average crystallite diameter and the phase of the samples, X-ray powder diffraction (XRD) spectra were measured with a D8 Bruker Advanced AXS GmbH X-ray diffractometer using Cu *Ka* radiation at a wavelength of 0.154056 nm. The measurement conditions were as follows: the wavelength was 0.15419 nm (pure Cu Kα radiation), tube voltage/tube current was 40 kV/50 mA, and machine scanning range was $2\theta = 10^0$- 90^0. The size and morphology of the as-prepared particles were carried out by using a scanning electron microscope (SEM), Tescan VEGA 3 SEM. The photoluminescence (PL) spectrum as well as decay curves for all the samples were investigated by Cary Eclipse fluorescent spectrophotometer equipped with a 150 W xenon lamp at an excitation source with the slit of 1.0 nm and scan speed of 240 nm min^{-1}.

III. Results And Discussions

3.1 X-ray diffraction study

Fig. 1 illustrates the X-ray diffraction patterns of Y_2O_3:Eu^{3+}: Ho^{3+} powder samples, synthesized by the sol–combustion method. Six main peaks are observed, which can be assigned to (211), (222), (400), (440), and (622) of cubic Y_2O_3. All diffraction peaks are attributed to the pure body-centered cubic (bcc) structure for Y_2O_3 phase and match well with JCPDS (25-1200) card with space group Ia3. All samples present (222) as the preferential orientation. At 0.1% Ho^{3+}, the product is already crystallized and presents some three peaks. At higher concentrations more peaks are detected. This difference in crystallization is due probably to the difference in the Ho^{3+} ions concentrations. Increasing Ho^{3+}% ions leads to the increase of the main peaks intensity with a sharpening, indicating the improvement of the crystallinity quality of the powders. This phenomenon can be explained by the fact that the Y^{3+} ions are accommodated in two different symmetries, i.e., the C_2 without inversion center and the S_6 with inversion center [24]. The Eu^{3+} ion might be replacing the Y^{3+} ions in theY_2O_3 host lattice because no diffraction pattern characteristic of Eu_2O_3 phase is detected. The radii of Y^{3+}, Eu^{3+} and Ho^{3+} ions are 0.89 A° , 0.947 A° and 0.9 A° respectively,[24]. According to the ion radius approximation principle in the crystal field theory, Eu^{3+} and Ho^{3+} ions enter into crystal lattices by replacing Y^{3+} ions other than by occupying the slot between crystal lattices. Compared with Y^{3+} ionic radius (0.89 Å), Eu^{3+} and HO^{3+} have larger ionic radii of 0.947 Å and 0.9 Å respectively. Therefore, the lattice constant would increase with increasing atomic content of Ho^{3+} ions in the powder.

The crystallite size of these materials has been estimated from the same XRD patterns. As a first approximation, it is suggested that the appearance of broad XRD peaks is due to the nano-sized particles formation. The average crystallite size 'D' of Y_2O_3:Eu^{3+}: Ho^{3+} powders can be estimated using Scherrer's formula [25],

$$D = \frac{0.9\lambda}{\beta cos\theta}$$

where λ=1.5406 Å is the wavelength of the X-ray radiation used, β is the full width at half maximum (FWHM) of the (222) diffraction peak in the XRD patterns in radians, θ is the Bragg diffraction angle.

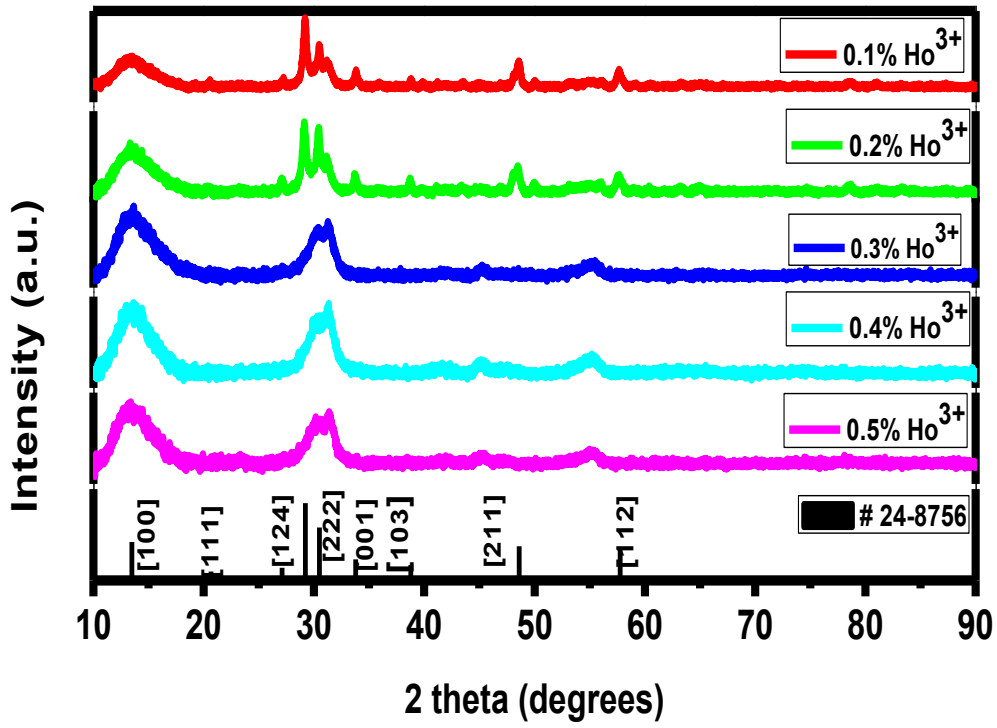

The average crystallite size and crystallographic unit cell parameters are calculated and listed in Table 1. It is found that the diffraction peaks shift to longer angles with increasing Ho%, indicating a decrease of the lattice constant and a development of internal tensile strain. In addition, the crystallite size of synthesized Y_2O_3: Eu^{3+}: Ho^{3+} powder increased with increasing Ho^{3+} ions. It is known that FWHM (β in the Scherrer formula) can be interpreted in terms of lattice strain and crystalline size. The crystal lattice strain generated by the Ho^{3+} ions is determined f

Fig.1. X-ray diffraction pattern of Y_2O_3: Eu^{3+}: Ho^{3+} phosphor

$$\beta \frac{cos\theta}{\lambda} = \frac{1}{D} + \eta sin\theta$$

where β is the full width at half maximum, λ is the X-ray wavelength, θ is the diffraction angle, D is the effective crystallite size and η is the effective strain. The strain is calculated from the slope of the plot of β ((cos θ)/λ) against sin θ/λ and the effective crystallite size is calculated from the intercept to β ((cos θ)/λ) axis. They show a difference in angular dependence of the line width for Ho^{3+} ions. Indeed, the best fit is obtained when the Ho^{3+} ion percent is increased from 0.1 to 0.5% and when the slope becomes negative. In the same table, we also present the effective crystallite size and the effective strain η against the Ho^{3+} ions percent. The effective crystallite size values are very close to those extracted from the Scherrer formula and increase when the Ho^{3+} ions percent increases. The tensile strain decreases from 0.1% to the negative value corresponding to 0.5%. It has been reported that a negative value indicates the presence of compressive lattice strain [28, 29]. This strain behaviour as a function of Ho^{3+} ions is in a good agreement with that of the lattice parameters. The reduction of the lattice parameter and the increase of crystallite size with increasing of the Ho^{3+} ions signify the closeness of lattice plane which can lead to an increase of the density and a decrease in the dislocation density. The average nanocrystallite sizes for Y_2O_3: Eu^{3+} with different concentration of HO^{3+} is compared as shown in the table 1 below;

Table 1. The crystallite sizes as a function of % concentration of HO^{3+} ions ions.

% of Ho^{3+}	0.1	0.2	0.3	0.4	0.5
Crystal sizes (nm)	6.5	7.5	8.9	9.2	9.8

Table 1 lists the crystallite sizes of synthesized particles estimated from the well-known Scherrer's equation. The diffraction data of the strongest peak [222] plane was used to calculate the mean crystallite sizes. The crystallite sizes showed a slightly increasing tendency, which can be attributed to the effect of the increased dopant concentration [30].

Figure 2 shows the role of Ho^{3+} mole concentration on crystallite sizes and lattice parameter. A monotonous decrease of the lattice constant and increasing crystallite size is established by means of X-ray analysis for a series of Y_2O_3: Eu^{3+}: Ho^{3+} powders. This effect cannot be explained by impurity or intrinsic defects in the powders. The expressions derived are based on the size dependence of the internal stress and the intracrystalline pressure stipulated by the interaction of the elements of the crystal charge lattice. Calculations made for the ion charge lattice of quartz evidence the monotonous increase of the lattice parameters with decreasing particle size and agree with the results of the X-ray experiment.

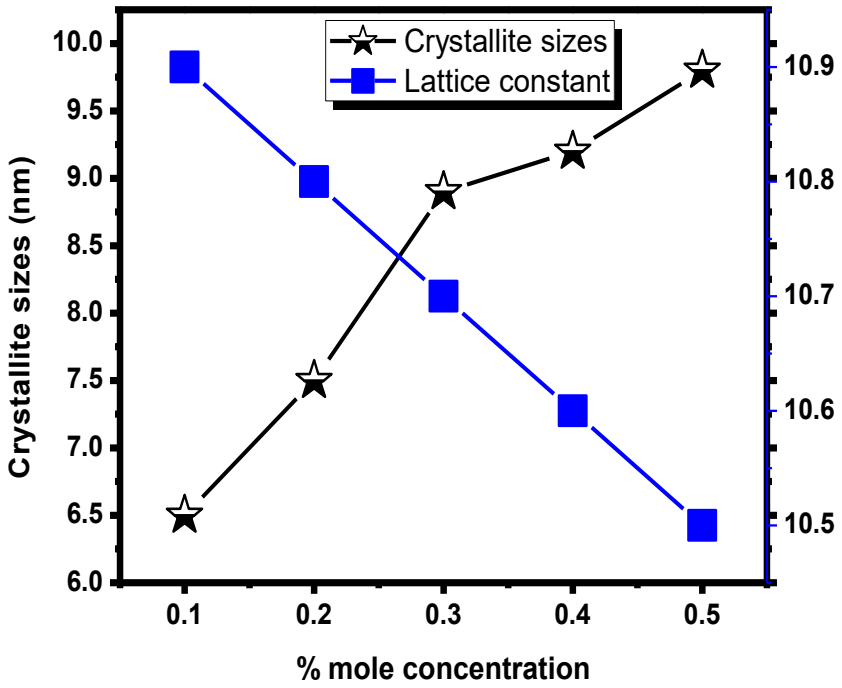

Fig. 2. Crystallite sizes and Lattice constant as functions of Ho^{3+} concentration

3.2 Scanning electron microscopy

SEM was carried out using Tescan VEGA 3 SEM. Fig. 3 shows the SEM image of the Y_2O_3:Eu^{3+}: Ho^{3+} co-doped phosphor. The image shows the characteristics surface morphology of combustion product. Particles are highly agglomerated and form a connected network type with some vacant space among them, which is expected due to the evolution of different gases during combustion of the gel. It also reveals inhomogeneous distribution of the particles (a variation and shape of the particles). The shape of some of the particles are spherical and the size lie between 5 – 10 nm (Fig.2a) which is well in agreement with the crystalline size calculated using XRD. However some particles are of sub-micron size due to agglomeration of many crystallites and lack of separate boundary (Fig.2b-2e). The shapes of the particles are irregular and seem to be polygonal.

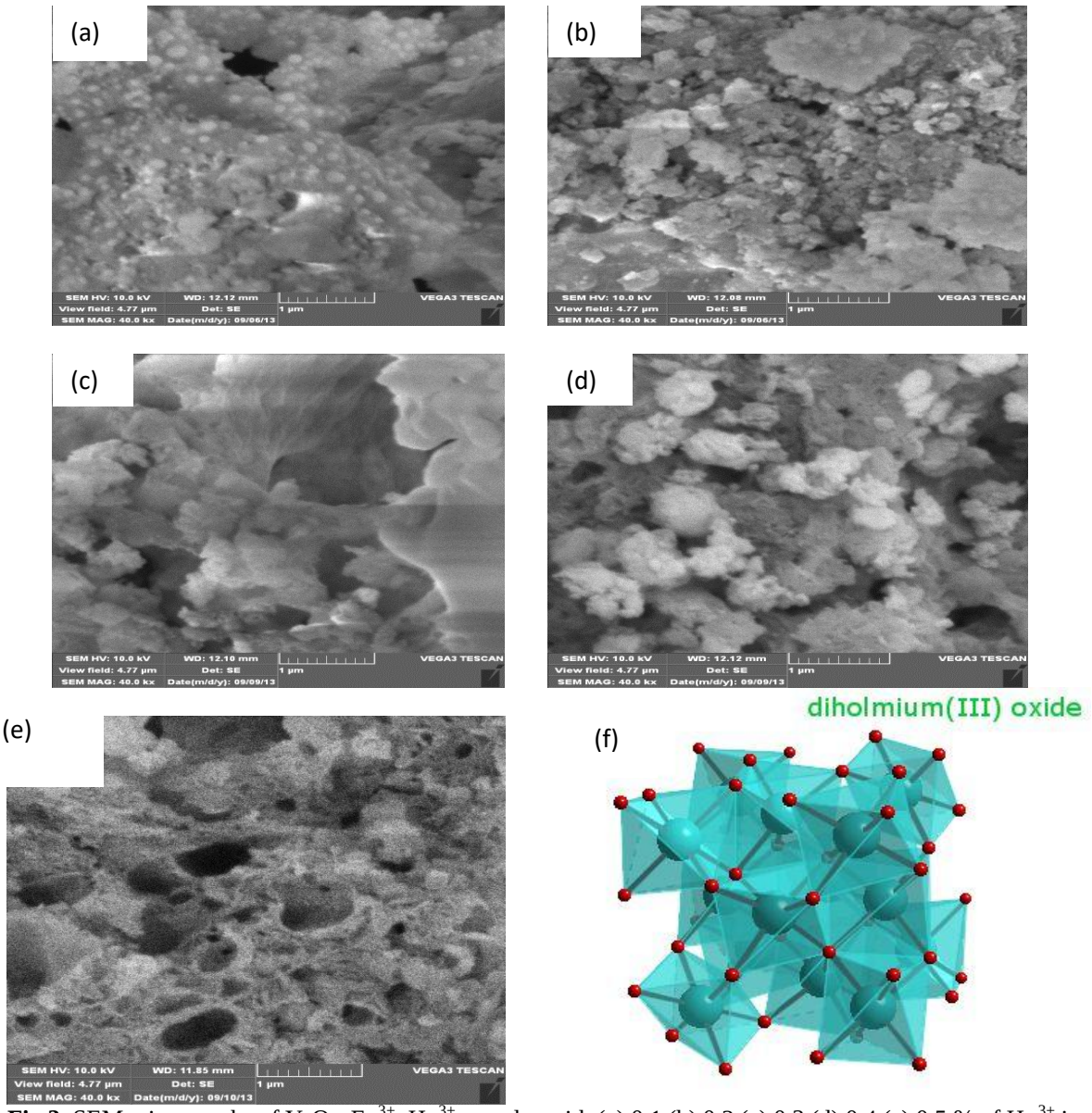

Fig.3. SEM micrographs of Y_2O_3: Eu^{3+}: Ho^{3+} samples with (a) 0.1 (b) 0.2 (c) 0.3 (d) 0.4 (e) 0.5 % of Ho^{3+} ions at 4.77µm field of view (f) Crystal structure of Ho_2O_3. Courtesy of ChemSpider.

IV. Photoluminescence

4.1 Excitation

Fig. 4 shows room-temperature optical absorption spectra of Y_2O_3:Eu^{3+}:Ho^{3+} phosphor. Ho^{3+} absorption bands of $^3H_6$, $^5G^5$, $^5G^6$, $^5F_3$, $^5F_4$ ($^5S_2$) and $^5F_5$ were present in Y_2O_3: Eu^{3+}:Ho^{3+}. The Ho^{3+} doped Y_2O_3:Eu^{3+} showed green (544 nm) and red (626 nm) emission peaks, which are assigned to $^5F_4$ ($^5S_2$) - $^5I_8$ and $^5F_5$-$^5I_8$ transitions of Ho^{3+} ions respectively.

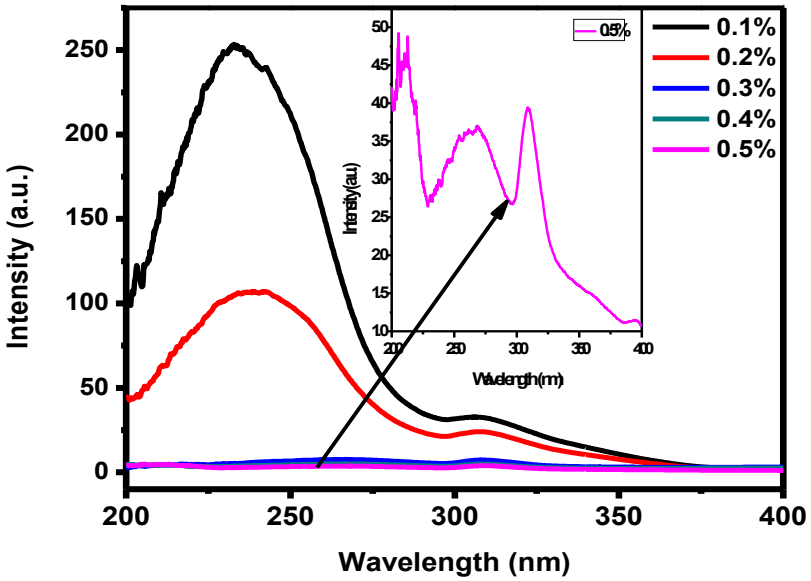

Fig.4 Excitation spectra of Ho^{3+} co-doped Y_2O_3: Eu^{3+} phosphor when Ho^{3+} ion concentration was varied from 0.1 to 0.5%

3.2 Emission

Fig. 5 shows the emission spectra of Y_2O_3: Eu^{3+}:Ho^{3+} powder when the percentage concentration of Ho^{3+} ions was varied. Three main emission spectra appear at 540, 588 and 626 nm for the samples with lower mole concentrations (0.1 and 0.2%) of Ho^{3+} assigned to $^5D_0$-$^7F_1$, $^5D_0$-$^7F_2$ and $^5D_0$-$^7F_3$ transitions of Eu^{3+}. These emission spectra due to Eu^{3+} ions are also confirmed by the inset of Fig. 3. Other minor peaks also appear around 440 and 500 nm speculated to be from Ho^{3+}. At higher mole concentration of Ho^{3+}, the three main peaks are totally quenched. Y_2O_3:Eu^{3+}:Ho^{3+} phosphor shows a red-emitting afterglow phenomenon, and the Eu^{3+} ions are the luminescent center during the decay process. The bright red emission near 626 nm has been noticeable due to the $^5D_0$-$^7F_2$ transition of Eu^{3+}. The Intensity of the luminescence has decreased with an increase of concentration of Ho^{3+}. In sufficient quantities of Eu^{3+} to Ho^{3+}, the bright red emission near 626 nm has been predominant due to $^5D_0$-$^7F_2$ transition of Eu^{3+}. From the figure, the intensities of spectra are quenched as the % concentration of Ho^{3+} ions are increased. Since Eu^{3+} ions are kept constant, it is speculated that Ho^{3+} ions are the ones which caused the quenching of the intensities of the spectra.The enhancement of the Eu^{3+} emission in the nanopowders is due to a non-radiative energy transfer from Ho^{3+} to Eu^{3+}, as Ho can absorb more X-ray radiation. At higher Ho^{3+} concentrations, a self-quenching mechanism [31] exists, a product of the fact that the Ho-Ho energy transfer mechanism is more efficient than the Ho-Eu one, and, therefore, presents a higher possibility that a Ho ion is closer than another sort, resulting in a drop in Eu^{3+} emission. Similar results have been observed for Gd_2O_3 co-doped Eu, Tb nanopowders [32].

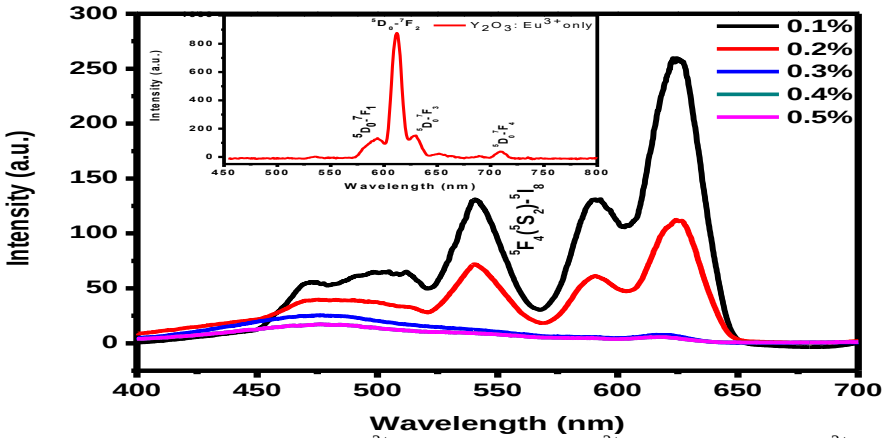

Fig.5. Photoluminescence emission spectra of Ho^{3+} co-doped Y_2O_3: Eu^{3+} phosphor when Ho^{3+} ion concentration was varied from 0.1 to 0.5%

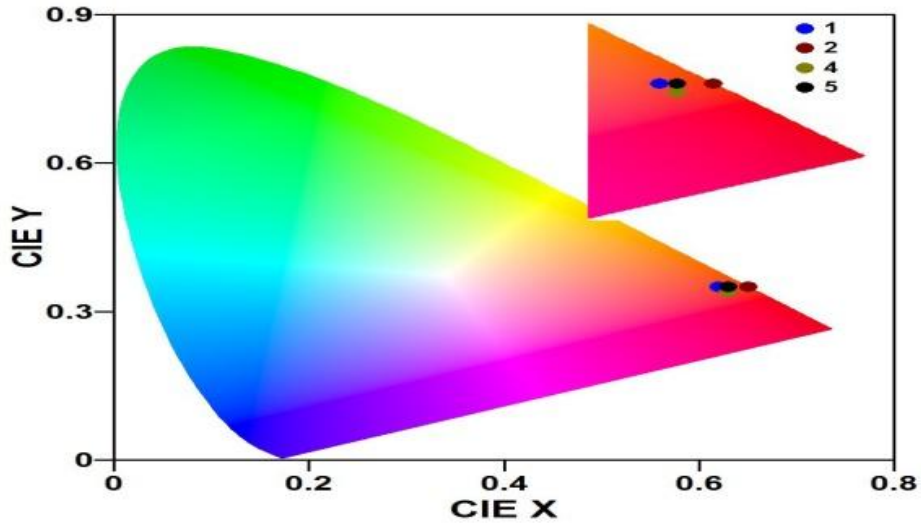

Fig.6. CIE diagram of the Y_2O_3:Eu^{3+}:Ho^{3+} powder under 325 nm UV excitation.

Fig.6. Illustrâtes the Commission Internationale de l'Eclairage (CIE) chromaticity diagram of Y_2O_3:Eu^{3+}:Ho^{3+}_x, ($0.1 \leq x \leq 0.5$) calculated using photoluminescence data and color calculator software. The coordinates shows the emissions were in orange/red region at 612 nm NBE for the samples with low mole percent of Ho^{3+}. Thus, this indicates that careful choice of dopant play a major role in tuning the emission color of the Y_2O_3:Eu^{3+}:Ho^{3+}.

3.3 Decay characteristics

The afterglow properties of Y_2O_3: Eu^{3+}: Ho^{3+} powder with different mole concentration of Ho^{3+} ions are shown in Fig. 7. It can be seen that decay curve of the powders with lowest concentrations has highest intensities and afterglow, while those with higher mole concentration of Ho^{3+} ions has the lowest intensities and . This indicates that lower mole concentration of Ho^{3+} favors long afterglow and higher intensities and vice versa. The decay times of the phosphor can be estimated by using the following double exponential equation;

$$I = A_1 \exp(-t/\tau_1) + A_2 \exp(-t/\tau_2)$$

where I is the phosphorescence intensity, A_1, and A_2, are constants, t is time, τ_1 and τ_2, are decay times for exponential components, respectively. The fitting results of parameters t_1 and t_2 are listed in Table 2 below;

% concentration	**0.1**	**0.2**	**0.3**	**0.4**	**0.5**
Components	**Decay constants(τ, s)**				
Fast (τ_1)	0.368	0.352	0.345	0.339	0.326
Medium (τ_2)	0.680	0.668	0.641	0.625	0.599

Table 2: Decay constants for the fitted decay curves of the Y_2O_3: Eu^{3+}:Ho^{3+} powder with various mole concentration.

The graph of maximum peak intensity of the as-prepared powders as a function of % Ho^{3+} concentration is shown in Fig.8. The emission peak intensity quenched gradually with increase in the % concentration of Ho^{3+} ions. It can be seen from the curve that the powders showed differences in initial intensity and medium persistence when the powders were efficiently activated by UV lamp. The results indicate that the initial luminescence intensity and the decay time of phosphors are enhanced with a decrease in the % concentration.

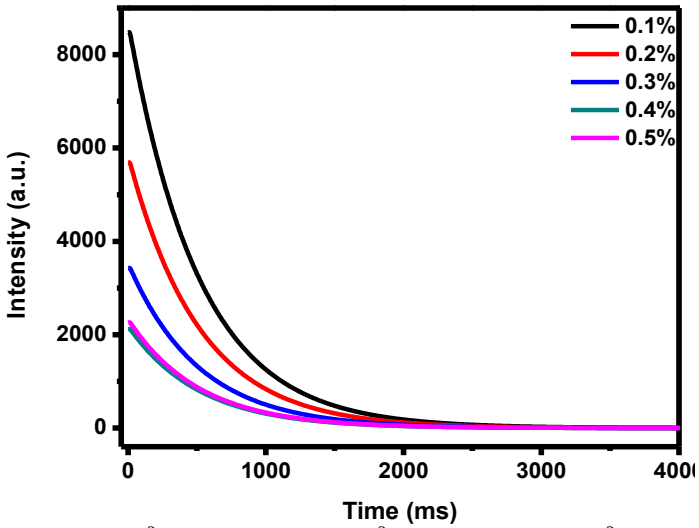

Fig.7. Decay curves of Ho^{3+} co-doped Y_2O_3: Eu^{3+} phosphor when Ho^{3+} ion concentration was varied from 0.1 to 0.5%

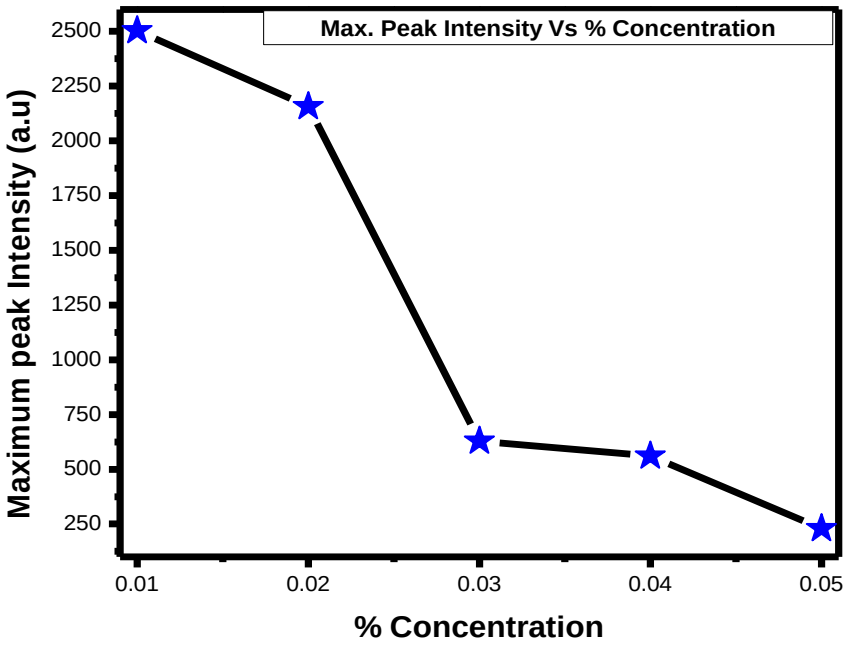

Fig.8. Concentration of Ho^{3+} ions vs. maximum peak intensity graph of Y_2O_3:Eu^{3+}:Ho^{3+} phosphor

3.4 Optical properties

3.4.1 Absorbance spectra

The UV–vis absorbance spectra of the samples are given in Fig. 9. The spectra of all the powder samples show good optical quality in the visible range due to the complete absorbance in the 200– 700 nm range. The sharp absorption edge is characteristic of a homogeneous structure [33]. The figure shows that the absorption edge shifted to higher wavelength for higher mole concentration and then reduced to lower wavelength for lower mole concentration. Furthermore, absorption bands corresponding to the forbidden Eu^{3+} f–f transitions were detected for higher mole concentration. The band at around 220 and330 nm is attributed to the exciton absorption, which is red-shift, compared with powder Y_2O_3:Eu^{3+}:Ho^{3+} [34]. The absorption peaks at around 290 and 340 nm are assigned to ^5Do-$^7F_1$and $^5D_0$-$^7F_2$ transitions of Eu^{3+} ions, respectively [35].

4.2 Determination of Eg. from reflectance spectra

The Kubelka- Munk equation was used to calculate the band gap of the as- prepared powder as follows;

$$F(R\infty) = \frac{(1-R\%)^2}{2R\%} = k/s \text{----------} \quad (1)$$

Where $R_\infty = R_{sample}/R_{references}$, K is absorption coefficient and S is scattering coefficient.
On the other hand the bang gap Eg, and absorption coefficient α of indirect band gap semiconductor are related through the well- known Tauc relation;

$$\alpha h\nu = C_1(h\nu - E_g)^2 \text{---------- (2)}$$

Where hν is the photo energy and C_1 is proportionality constant, n=2 for indirect transition. When the material scatters in a perfectly manner, the absorption coefficient K becomes equal to 2α (K=2α). Considering the scattering coefficient S as constant with respect to wavelength, and using equations (1) and (2), the following expression can be written:

$$[F(R\infty) * h\nu]^2 = C_2(h\nu - E_g) \text{---------- (3)}$$

By plotting $[F(R)*h\nu]^2$ against hν and fit the linear region with a line and extend it to the energy axis, then one can easily obtain E_g by extrapolating the linear regions to $[F(R_*)\ h\nu]^2=0$. The average Eg. value for the powders was found to be 4.43 eV, which is in a good agreement with the literature values by other researchers [36]. The observed optical bang gap for Y_2O_3: Eu^{3+}:Ho^{3+} samples have decreased to 4.0 eV at lower mole concentration of Ho^{3+} shown in Fig. 10. The change in optical band gap values may also be due to the change of crystal structure of the Y_2O_3 powders. This change in the optical band gap materials can be explained on the basis of quantum size effect.

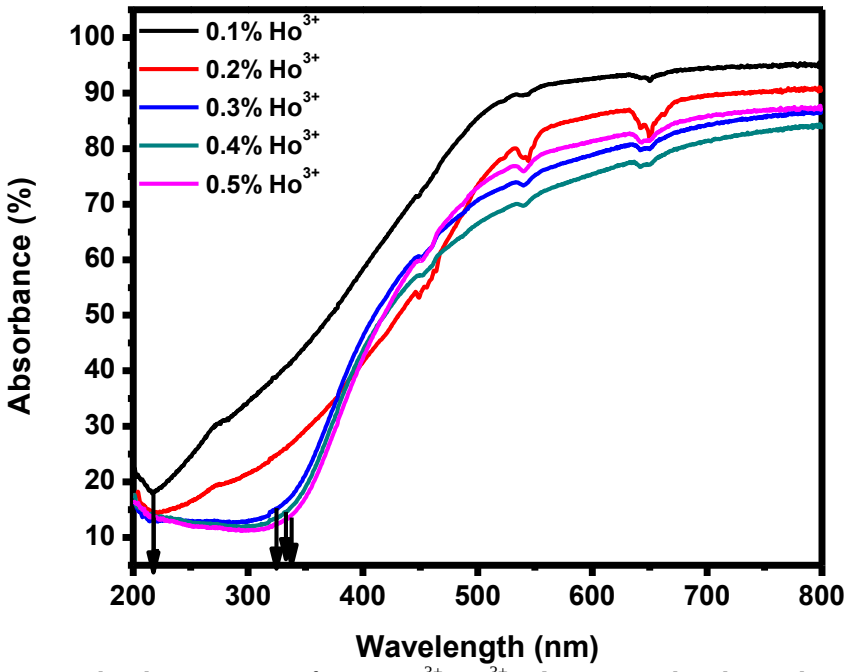

Fig 9. Uv-vis absorbance spectra of Y_2O_3: Eu^{3+}: Ho^{3+} red- emitting phosphor with % mole concentration of Ho^{3+} from 0.1 to 0.5%.

The dependence of the band gap energy of the Y_2O_3:Eu^{3+}:Ho^{3+} on the percent mole concentration of Ho^{3+} ions is shown in Fig. 11. It can be seen from the graph that the band gap of the Y_2O_3; Eu^{3+}: Ho^{3}+ powders increased with the percent mole concentration of Ho^{3+}. The decrease in band gap energy and the shift of the absorption edges to higher wavelengths might be due to the presence of defect states and disorder due to the percent mole concentration. The mole concentration of Ho^{3+} might have introduced new states close to the conduction band of the Y_2O_3:Eu^{3+}: Ho^{3+}. A new defect band is therefore formed below the conduction which lead to reduction in the effective band gap [37, 38]. It is clear that at 0.5% mole concentration of Ho^{3+} the estimated band gap increased upto 4.7 eV.

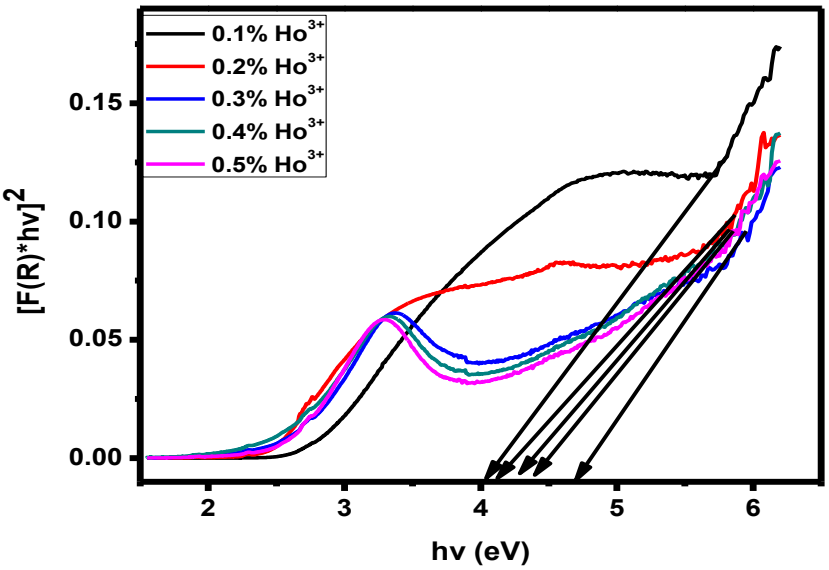

Fig.10. Graph of F [(R)*hv] ^{2} as a function of band gap energy

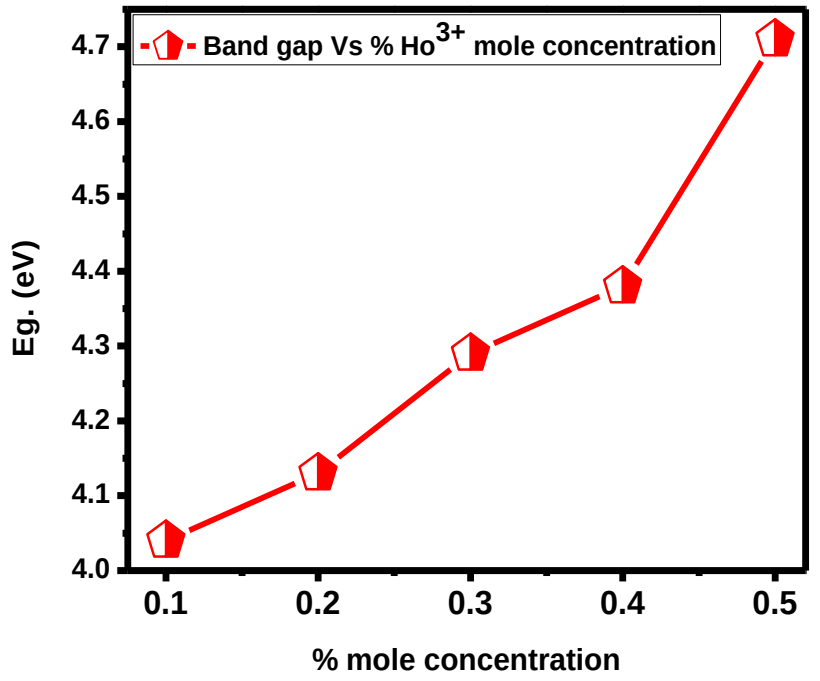

Fig. 11. Band gap energy as a function of Ho^{3+} mole concentration

V. Conclusion

We have successfully synthesized co-doped Y_2O_3:Eu^{3+}:Ho^{3+} powders by simple and cost effective sol-combustion method. The effects of Ho doping on the structure and optical properties of Y_2O_3:Eu^{3+} are investigated. X-ray diffraction confirm the formation of body-centred cubic structure of Y_2O_3: Eu for all Ho concentration. The SEM images and XRD shows that the crystallite sizes increase with increase in Ho concentration. The PL spectra show strong and narrow visible light emission outspreading from 450 to 650 nm which is frequently observed in alloy semiconductors. The UV–vis spectroscopy study reveals that the optical band gap (Y_2O_3:Eu^{3+}:$Ho^{3+}{}_x$, $0.1 \leq x \leq 0.5$) alloys show red-shift. Ho-codoping can effectively adjust and tune Y_2O_3:E^{3+} for narrow band gap applications. In summary, we suggest that the method employed would be efficient to synthesize material for devices operating in the visible region as well as for developing heterojunction structures.

Acknowledgements

This work was supported by the University of the Free State (UFS) and National Research Foundation (NRF) of South Africa. The authors kindly acknowledge department of Physical Sciences, Meru University of Science and Technology (MUST) for their support.

References

[1]. X. Zhang, C. Serrano, E. Daran, F. Lahoz, G. Lacoste, A. Munoz-Yagüe, Phys. 2000, Rev. B 62: 4446.
[2]. L.F. Johnson, H.J. Guggenheim, Appl. Phys.1971, Lett. 19: 44.
[3]. S. Ray, P. Pramanik, A. Singha, A. Roy, J. Appl. Phys.2005, 97: 094312-1.
[4]. M.-F. Joubert, Opt. Mater. 1999, 11: 181.
[5]. X.X. Luo, W.H. Cao, Mater. Lett. 2007, 61: 3696.
[6]. R. Schmechel, M. Kennedy, H. Von Seggern, H. Winkler, M. Kolbe, R.A. Fischer, L. Xaomao, A. Benker, M. Winterer, H. Hahn, J. Appl. Phys.2001, 89: 1679.
[7]. H.W. Song, B.J. Chen, H.S. Peng, J.S. Zhang, Appl. Phys. 2002, Lett. 81: 1776.
[8]. X.M. Li, A. Benker, M. Winterer, H. Hahn, J. Appl. Phys. 2001, 89: 1679.
[9]. G.Y. Hong, K. Yoo, S.J. Moon, J.S. Yoo, J. Electrochem. Soc. 2003, 150: H67.
[10]. G. Wakefield, E. Holland, P.J. Dobson, J.L. Hutchison, Adv. Mater. 2001, 20: 1557.
[11]. H. Peng, H. Song, B Chen, S. Lu, S. Huang, Chem. Phys. Lett. 2003, 370: 485.
[12]. K .Y. Jung, C. H. Lee, Y. C. Kang, Mater. Lett. 2005, 59: 2451.
[13]. T. Jüstel, H. Nikol, and C. Ronda, "New developments in the field of luminescent materials for lighting and displays," Angewandte Chemie. 1998, vol. 110: pp. 3250–3271.
[14]. A. L. Rogach, N. Gaponik, J. M. Lupton et al, "Light-emitting diodes with semiconductor nanocrystals," Angewandte Chemie. 2008, vol. 47, no. 35: pp. 6538–6549.
[15]. M. Dahan, T. Laurence, F. Pinaud et al, "Time-gated biological imaging by use of colloidal quantum dots," Optics Letters, 2001, vol. 26, no. 11: pp. 825–827.
[16]. K. E. Gonsalves, G. Carlson, S .P. Rangarajan, M. Benaissa, and M. José-Yacamán, "Synthesis and characterization of a nanostructured gallium nitride-PMMA composite," Journal of Materials Chemistry, 1996, vol. 6, no. 8: pp. 1451–1453.
[17]. R. G. Pappalardo and R. B. Hunt, "Dye-laser spectroscopy of commercial Y_2O_3:Eu^{3+} phosphors," Journal of the Electrochemical Society, 1985, vol. 132: pp. 721–730.
[18]. C. R. Ronda, "Phosphors for lamps and displays: an applicational view," Journal of Alloys and Compounds, 1995, vol. 225, no. 1-2: pp. 534–538.
[19]. T. Justel, H. Nikol, and C. Ronda, "New development in the field of luminescent materials for lighting and displays," Angewandte Chemie. 1998, vol. 37: pp. 3084–3103.
[20]. X. Jing, T. Ireland, C . Gibbons et al, "Control of Y_2O_3: Eu spherical particle phosphor size, assembly properties, and performance for FED and HDTV," Journal of the Electrochemical Society, 1999, vol. 146, no. 12: pp. 4654–4658.
[21]. C. H Kim, I .E. Kwon, C .H. Park et al, "Phosphors for plasma display panels," Journal of Alloys and Compounds, 2000, vol. 311, no. 1: pp. 33–39.
[22]. F. Lahoz, I.R. Martin, J.M. Calvilla-Quintero, Appl. Phys. Lett. 2005, 86.
[23]. M. Malinowski, A. Wnuk, Z. Frukacz, G. Chadeyron, R. Mahiou, S. Guy, M.F. Joubert, J. Alloys Compd. 2001, 323: 731.
[24]. M. Malinowski, M. Kaczkan, A. Wnuk, M. Szuflinska, J. Lumin. 2004, 106: 269.
[25]. W. W. Zhang, M. Xu, W. P, Zhang et al, "Site-selective spectra and time-resolved spectra of nanocrystalline Y_2O_3:Eu^{+3}," Chemical Physics Letters, 2003, vol. 376, no. 3-4: pp. 318–323.
[26]. X. Qin, T. Yokomori, Y. Ju. Flame synthesis and characterization of rare-earth (Er^{3+}, Ho^{3+}, and Tm^{3+}) doped upconversion phosphors. Appl Phys Lett. 2007, 90:073104 : Doi: 10.1063/1.2561079.
[27]. D. Tu, Y. Liang, R. Liu, D. Li. Eu/Tb ions co-doped white light luminescence Y_2O_3 phosphors. J Lumin. 2011, 131:2569-2573: Doi: 10.1016/j.jlumin.2011.05.036.
[28]. H. Wang, J. Yang, C.M. Zhang, J. Lin, Synthesis and characterization of monodisperse spherical Sio_2:RE_2O_3 (RE=rare earth elements) and SiO_2:Gd_2O_3:Ln^{3+} (L_n=Eu, Tb, Dy, Sm Er,Ho) particles with core shell structure. J solid Stae Chem. 2009, 182:2716-2724: Doi: 10.1016/j.jssc.2009.07.033.
[29]. M. A. Flores-Gonzales, G. Ledoux, S. Roux, K. Lebbou, P. Perriat, O. Tillement, Preparing nanometer scaled Tb-doped Y_2O_3 luminescent powders by the polyol method. J Solid State Chem 2005, 178:989-997.
[30]. T.S Atabaev, J.H Lee, D.W Han, Y-H Hwang, H-K Kim, Cytotoxicity and cell imaging potentials of submicron color-tunable yttria particles. J Biomed Mat Res A 2012, 100(9):2287-2294
[31]. S. Mukherjee, V. Sudarsan, R.K. Vatsa, S.V. Godbole, R.M. Kadam, U.M. Bhatta, A.K. Tyagi. Effect of structure, particle size and relative concentration of Eu3+ and Tb3+ ions on the luminescence properties of Eu^{3+} co-doped Y_2O_3: Tb nanoparticles. Nanotechnology 2008, 19: 325704–325711.
[32]. A. de J. Morales-Ramírez, A. García-Murillo, F.de J. Carrillo-Romo, M. García-Hernández, D. Jaramillo-Vigueras, G. Chaderyron, D. Boyer. Properties of Gd_2O_3:Eu^{3+}, Tb^{3+} nanopowders obtained by sol-gel process. Mater. Res. Bull. 2010, 45: 40–45.
[33]. Q. Pang, J. Shi, Y. Liu, D. Xing, M. Gong, N. Xu, Mater. Sci. Eng. 2003, B 103: 57.
[34]. M. Kaczkan, M. Malinowski, J. Alloys Compd. 2004, 380: 201.
[35]. J.C. Park, H.K. Moon, D.K. Kim, S.H. Byeon, B.C. Kim, K.S. Suh, Appl. Phys. Lett. 2000, 77: 2162.
[36]. T.S Atabaev, H-HT Vu, Z. Piao, H-K Kim, Y-H Hwang, Tailoring the luminescent properties of co-doped Gd_2O_3:Tb^{3+} phosphor particles by co-doping with Al^{3+} ions. J Alloys Compd 2012, 541:263-268.
[37]. J.L. Ferrari, A.M. Pires, M.R. Davolos, Mater. Chem. Phys. 2009, 113: 587.
[38]. K.L. Nash, R.C. Dennis, N.J. Ray, J.B. Gruber, D.K. Sardar, J. Appl. Phys. 2009, 106.

Abdub G. Ali Narrow Visible Emission And Narrowing Band Gap In Ho3+-Co Doped Y2O3: Eu3+ Nanopowders Prepared Via Sol- Combustion Route." IOSR Journal of Applied Physics (IOSR-JAP) , vol. 9, no. 6, 2017, pp. 23-33.